

Feasibility analysis for acquiring visibility based on lidar signal using genetic algorithm-optimized back propagation algorithm

Guo-Dong Sun(孙国栋), Lai-An Qin(秦来安), Zai-Hong Hou(侯再红), Xu Jing(靖旭), Feng He(何枫), Feng-Fu Tan(谭逢富), Si-Long Zhang(张巳龙), Shou-Chuan Zhang(张守川)

Citation: Chin. Phys. B . 2019, 28(2): 024213. **doi:** 10.1088/1674-1056/28/2/024213
Journal homepage: http://cpb.iphy.ac.cn; http://iopscience.iop.org/cpb

What follows is a list of articles you may be interested in

Detection performance improvement of photon counting chirped amplitude modulation lidar with response probability correction

Yi-Fei Sun(孙怿飞), Zi-Jing Zhang(张子静), Li-Yuan Zhao(赵丽媛), Wei-Min Sun(孙伟民), Yuan Zhao(赵远)

Chin. Phys. B . 2018, 27(9): 094213. **doi:** 10.1088/1674-1056/27/9/094213

The intensity detection of single-photon detectors based on photon counting probability density statistics

Zijing Zhang(张子静), Long Wu(吴龙), Jie Song(宋杰), Yuan Zhao(赵远)

Chin. Phys. B . 2017, 26(10): 104207. **doi:** 10.1088/1674-1056/26/10/104207

A high precision phase reconstruction algorithm for multi-laser guide stars adaptive optics

Bin He(何斌), Li-Fa Hu(胡立发), Da-Yu Li(李大禹), Huan-Yu Xu(徐焕宇), Xing-Yun Zhang(张杏云), Shao-Xin Wang(王少鑫), Yu-Kun Wang(王玉坤), Cheng-Liang Yang(杨程亮), Zhao-Liang Cao(曹召良), Quan-Quan Mu(穆全全), Xing-Hai Lu(鲁兴海), Li Xuan(宣丽)

Chin. Phys. B . 2016, 25(9): 094214. **doi:** 10.1088/1674-1056/25/9/094214

V-L decomposition of a novel full-waveform lidar system based on virtual instrument technique

Xu Fan, Wang Yuan-Qing

Chin. Phys. B . 2015, 24(10): 104214. **doi:** 10.1088/1674-1056/24/10/104214

Comprehensive wind correction for a Rayleigh Doppler lidar from atmospheric temperature and pressure influences and Mie contamination

Shangguan Ming-Jia, Xia Hai-Yun, Dou Xian-Kang, Wang Chong, Qiu Jia-Wei, Zhang Yun-Peng, Shu Zhi-Feng, Xue Xiang-Hui

Chin. Phys. B . 2015, 24(9): 094212. **doi:** 10.1088/1674-1056/24/9/094212

Feasibility analysis for acquiring visibility based on lidar signal using genetic algorithm-optimized back propagation algorithm*

Guo-Dong Sun(孙国栋)[1,2], Lai-An Qin(秦来安)[2,†], Zai-Hong Hou(侯再红)[2], Xu Jing(靖旭)[2], Feng He(何枫)[2], Feng-Fu Tan(谭逢富)[2], Si-Long Zhang(张巳龙)[2], and Shou-Chuan Zhang(张守川)[2]

[1] *Key Laboratory of Atmospheric Optics, Anhui Institute of Optics and Fine Mechanics, Chinese Academy of Sciences, Hefei* 230031, *China*
[2] *Science Island Branch of Graduate School, University of Science and Technology of China, Hefei* 230031, *China*

(Received 13 July 2018; revised manuscript received 14 October 2018; published online 10 January 2019)

Visibility is an important atmospheric parameter that is gaining increasing global attention. This study introduces a back-propagation neural network method based on genetic algorithm optimization to obtain visibility directly using light detection and ranging (lidar) signals instead of acquiring extinction coefficient. We have validated the performance of the novel method by comparing it with the traditional inversion method, the back-propagation (BP) neural network method, and the Belfort, which is used as a standard value. The mean square error (MSE) and mean absolute percentage error (MAPE) values of the genetic algorithm-optimized back propagation (GABP) method are located in the range of 0.002 km^2–0.005 km^2 and 1%–3%, respectively. However, the MSE and MAPE values of the traditional inversion method and the BP method are significantly higher than those of the GABP method. Our results indicate that the proposed algorithm achieves better performance and can be used as a valuable new approach for visibility estimation.

Keywords: visibility, neural network, lidar signals, extinction coefficient

PACS: 42.68.Kh, 42.68.Wt, 42.79.Ta **DOI:** 10.1088/1674-1056/28/2/024213

1. Introduction

Visibility is an important atmospheric parameter that has attracted increased attention in recent years. The decline in atmospheric visibility caused by increased aerosol emissions has become an important environmental issue in China.[1] Low visibility is a dominant problem in areas close to airports, which affects aviation safety during take-off and landing. Low-visibility weather conditions also limit road traffic and lead to navigational accidents, especially in the narrow areas of straits or rivers. Consequently, detecting visibility is critical for transportation security. The most fundamental definition of visibility is a measure of the ability of unaided human eye to identify distant objects.[2] However, the visibility determined by subjective ground observers involves significant uncertainty and varies from person to person. With advances in technology, modern methods used to measure visibility rely primarily on instrumentation. For example, transmissometers (Vaisala, Finland) and scatterometers (Belfort, USA) have been used at airports and along highways. Light detection and ranging (lidar), as an active remote sensing technology, has been widely used in the areas of laser transmission, climate prediction, aerosol radiance force effects, and atmospheric environment measurements.[3,4] Several studies have investigated the potential application of lidar to visibility detection.[5–9] In this paper, we proposed a new method to acquire visibility based on lidar signal using genetic algorithm-optimized back propagation (GABP) algorithm. Our results are in good agreement with the data of Belfort meter, which indicates that the visibility can be obtained directly using our proposed approach without calculating the extinction coefficient.

2. Traditional lidar method for visibility detection

Each of the instruments described above calculates visibility from an acquired extinction coefficient. This paper focuses on the use of lidar to detect visibility, with instrumentation measurements (Belfort) assumed to be the standard value. The Klett and Fernald methods are commonly used to invert extinction coefficients based on a lidar signal.[3,10] In the Klett method used in this study, the extinction coefficients are represented as follows:[3]

$$\sigma(z) = \frac{\exp[(S - S_{\mathrm{m}})/k]}{\{\sigma_{\mathrm{m}}^{-1} + (2/k)\int_z^{z_{\mathrm{m}}} \exp[(S - S_{\mathrm{m}})/k]\,\mathrm{d}z'\}}. \quad (1)$$

where k depends on lidar wavelength and aerosol features (we assume $k = 1$), z is the lidar detection range, z_{m} is the detection range at the calibration point, σ_{m} is the extinction coefficient at the calibration point and the value of this point is acquired by Broyden algorithm,[11] S is the range-corrected lidar signal, and S_{m} is the range-corrected lidar signal at the calibration point. Figure 1 is the lidar system used in this study that is described by Sun *et al.*[12]

Figure 2 shows an experimental image in Hefei with high concentrations of aerosol particles illuminated in the air. The

*Project supported by the National Natural Science Foundation of China (Grant No. 41405014).
†Corresponding author. E-mail: laqin@aiofm.ac.cn
© 2019 Chinese Physical Society and IOP Publishing Ltd

lidar has excellent range resolution in the near region and could be suitable for visibility detection. The Belfort visibility meter measures extinction coefficients at small distances. We have calculated the visibility using the mean value of the first two extinction coefficients acquired from the lidar in order to approach the method used in the Belfort.

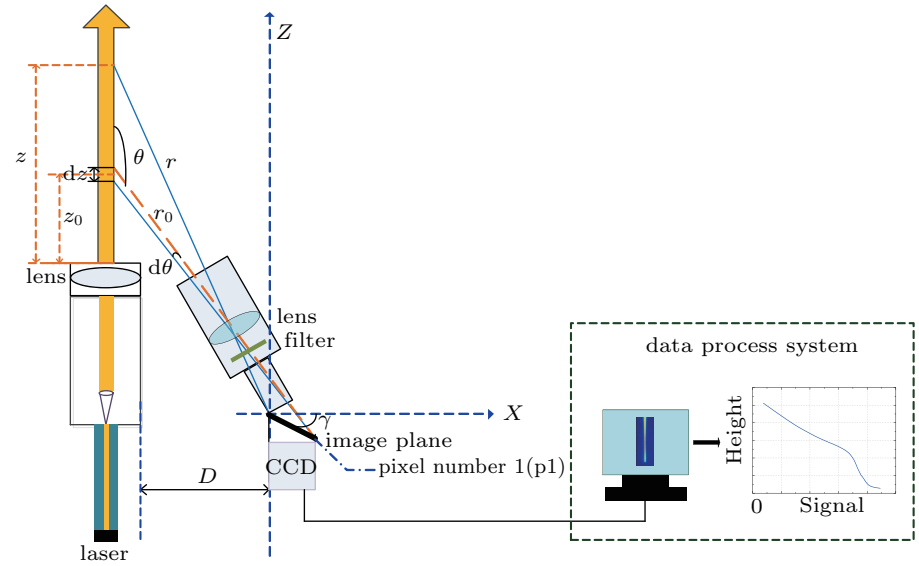


Fig. 1. Schematic diagram of lidar system.



Fig. 2. The experimental image.

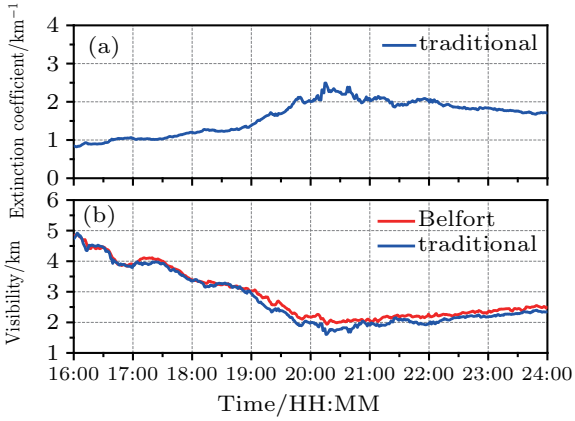


Fig. 3. Visibility obtained by the traditional method and Belfort.

The relationship between visibility and atmospheric extinction coefficients depends on the physical properties of the hydrometeor and the wavelength as follows:[13]

$$\sigma = \frac{3.912}{V}\left(\frac{\lambda}{550\ \text{nm}}\right)^{-q}. \tag{2}$$

where σ (in unit of km^{-1}) is the extinction coefficient, V (in unit of km) represents the visibility, λ (in unit of nm) denotes the detection wavelength, and q is an empirical correction factor given by

$$q = \begin{cases} 1.6 & (V > 50\ \text{km}), \\ 1.3 & (6\ \text{km} < V < 50\ \text{km}), \\ 0.16V + 0.34 & (1\ \text{km} < V < 6\ \text{km}), \\ V - 0.5 & (0.5\ \text{km} < V < 1\ \text{km}), \\ 0 & (V < 0.5\ \text{km}). \end{cases} \tag{3}$$

Finally, visibility is obtained using Eq. (2), as shown in Fig. 3.

3. New method for visibility detection

As demonstrated in Fig. 3, visibility detected using lidar is in excellent agreement with the Belfort measurements. This supports the viability of the lidar system and the accuracy of the acquired signal. However, some variables are replaced by empirical or hypothetical values for the convenience of calculation during inversion of the extinction coefficient, which introduces uncertainty and errors in the calculation.[3] The high degree of visibility similarity between lidar and Belfort suggests that a new method can be developed to calculate visibility without the need to invert extinction coefficients. We propose the use of a neural network model with autonomous learning functions for visibility calculation. By learning the sample patterns, the internal mechanisms between the information can be distributed and stored in the network. A back propagation (BP) neural network method, developed using steepest gradient descent, can then be used to solve for visibility. Its primary function is to modify the weights between layers to minimize total error in the network.[14] The network learning process is a backward propagation of errors, and the

process of updating the weights and threshold coefficients is constantly updated. However, the primary flaw of this BP algorithm is that it has a tendency to fall into local optimal solutions because the initial thresholds and weights are generally initialized to random numbers over a certain range.[15] The genetic algorithm (GA) is a highly-parallel and adaptive detection technique which was developed from the theory of biological evolution in nature.[16,17] GA can preserve highly adaptable environmental gene characteristics and eliminate low-adaptation genetic features by distinguishing individual genetic changes in the simulation of individual organisms. Consequently, we propose a genetic algorithm-optimized back propagation network for visibility calculation. The structure of the GABP method is described in Fig. 4.

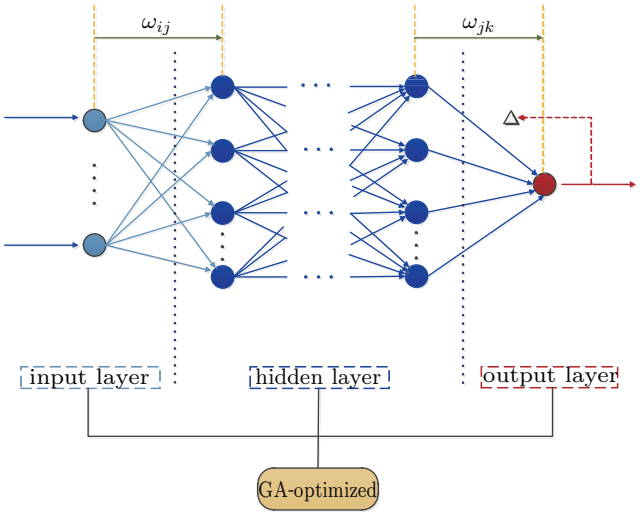


Fig. 4. The structure of the GABP neural network.

In the BP neural network, the signal is input through the input layer, calculated in the hidden layer, and results are obtained from the output layer. The output signal is then compared with the expected output value to calculate the corresponding error. The network is corrected from the back to the front based on the resulting error. During this process, the thresholds and connecting weights between layers are adjusted using the error gradient descent method. The process of weight adjustment for each forward propagation layer and back-propagation error is implemented periodically until the output error for the BP algorithm is below an acceptable level, as determined by the user or learning epochs established by the algorithm. The purpose of using GA to optimize the original thresholds and weights in the BP algorithm is to optimize the BP algorithm for improved output performance. Fundamentally, the network is represented by the original thresholds, individual weights, and calculation errors in the BP neural network, defining an individual fitness value. Optimal initial thresholds and weights are identified through selection, crossover, and mutation operations to identify the most suitable individual. This completes the network training process. In this study, GA is used to modify weights and thresholds in the BP algorithm, and GA can also be used to identify learning parameters and network structures.[15] A GABP flow chart is shown in Fig. 5.

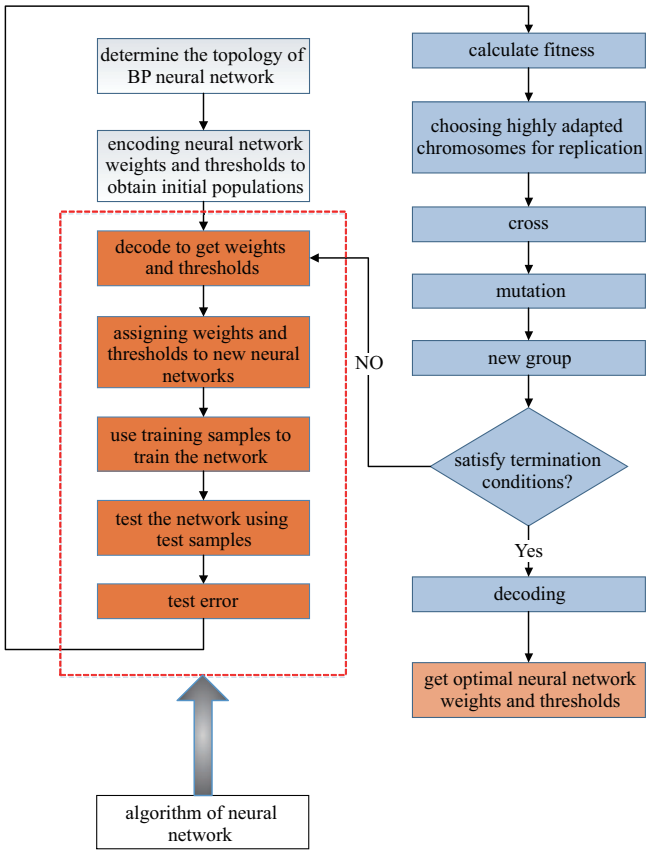


Fig. 5. A flow chart for GABP.

The network architecture is assumed to be n–s–m (n inputs, s neurons in the hidden layer, and m outputs). The term x_i represents the input signal, f_1 is the transfer function for the hidden layer, ω_{ij} represents the connection weight from the input layer to the hidden layer, and θ_j represents the threshold value of the hidden layer. The term b_j represents the output of the hidden layer, f_2 is the transfer function of the output layer, ω_{jk} indicates the connection weight from the hidden layer to the output layer, and θ_k represents the threshold value for the output layer. These values are used to produce the algorithm output y_k.[15] The output of the j_{th} neuron in the hidden layer is given by

$$b_j = f_1\left(\sum_{i=1}^{n} \omega_{ij} x_i - \theta_j\right) (i = 1,2,\ldots,n;\ j = 1,2,\ldots,s). \quad (4)$$

The output of the output layer can be expressed as

$$y_k = f_2\left(\sum_{j=1}^{s} \omega_{jk} b_j - \theta_k\right) (j = 1,2,\ldots,s;\ k = 1,2,\ldots,m). \quad (5)$$

The network training process involves continuously modifying the weights and thresholds to reduce the error between expected and output values until it is below a predefined goal

(0.009). The algorithm can also run a predetermined number of epochs (500). Lidar data are then inserted into the trained network and visibilities are acquired. This study incorporates four nodes in the input layer, representing two ranges and their corresponding intensities. The number of nodes in the hidden layer is determined using Eq. (6)[14]

$$N_2 = 2 \times N_1 + 1. \tag{6}$$

where N_1 and N_2 are the numbers of nodes in the input and hidden layers, respectively. The output layer contains one node representing visibility. The transfer function f_1 uses an S-type tangent function (tansig), while f_2 adopts an S-type logarithmic function (logsig).

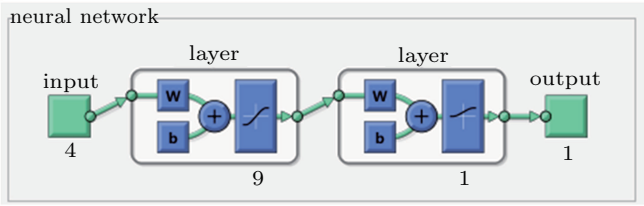


Fig. 6. A real neural network developed in Matlab.

Figure 6 shows a real neural network developed in Matlab. The first 300 sets of data shown in Fig. 3 are used as training data and the next 178 sets are used for calculative data. This program produces different results each time it runs thanks to the randomness of optimizing thresholds and weights in the GABP method. The results of the two consecutive runs are shown in Figs. 7 and 8. The visibility obtained by the GABP method, the traditional inversion method, the BP method, and the Belfort method are compared in the figures. There is a big difference between the traditional inversion method and the standard value. In addition, the correlation and absolute difference between visibility values obtained by GABP and BP methods and their standard values are acceptable.

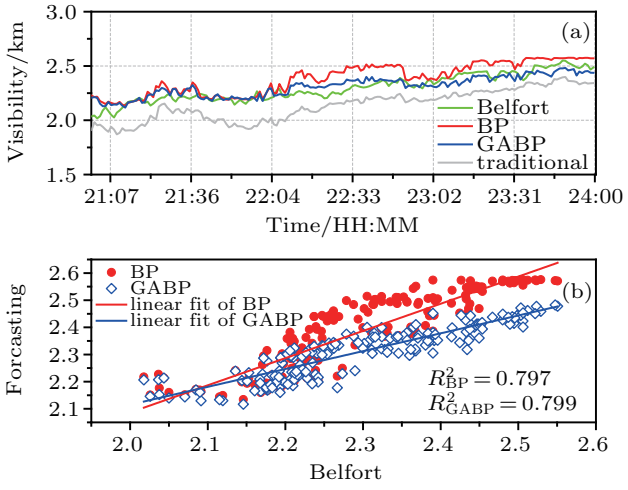


Fig. 7. A comparison between the BP and GABP methods for the first run.

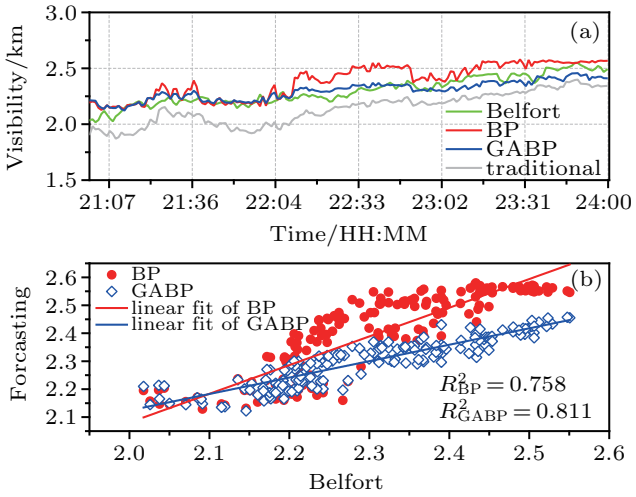


Fig. 8. A comparison between the BP and GABP methods for the second run.

The accuracy of these calculating results is quantitatively assessed using two performance functions: mean squared error (MSE) and mean absolute percentage error (MAPE). The corresponding expressions are as follows:[14]

$$\mathrm{MSE} = \frac{1}{N}\sum_{n=1}^{N}(y_n - \tilde{y}_n)^2, \tag{7}$$

$$\mathrm{MAPE} = \frac{1}{N}\sum_{n=1}^{N}\left|\frac{y_n - \tilde{y}_n}{y_n}\right| \times 100\%. \tag{8}$$

where y_n and $\tilde{y}_n$ represent the expected and calculating values for the n-th data, respectively, and N represents the total number of data used for performance evaluation and comparison.

Table 1. Two continuous runs.

	Method	MSE/km^2	MAPE /%
First run	BP	0.0116	3.9243
	GABP	0.0038	2.2134
	traditional	0.0285	7.0157
Second run	BP	0.0132	4.1305
	GABP	0.0040	2.3043
	traditional	0.0285	7.0157

Table 1 shows the results corresponding to the above two continuous operating conditions. Both the MSE and MAPE values for the traditional inversion and BP method are much higher than those of GABP, which demonstrates the viability of the GABP method. The program is then run one hundred times consecutively and the number of times MSE and MAPE appear in a range of numbers is tallied. Due to the fact that the traditional inversion results remain constant as the number of runs changes, we only show the relevant results of BP and GABP methods in Figs. 9 and 10. Figure 9 shows MSE values for the GABP method, which are all located in the range of 0.002 km^2–0.005 km^2. MSE values for the BP method are

significantly higher than those of the GABP method, with the highest MSE values in the range of 0.026 km^2–0.029 km^2. Figure 10 shows MAPE values for the GABP method, which are all located in the range of 1%–3%. MAPE values for the BP method are higher than those of the GABP method, with the highest MAPE values in the range of 6%–7%. Thus, the GABP method outperforms the BP method after sufficient optimization of weights and thresholds, and is also better than the traditional inversion method.

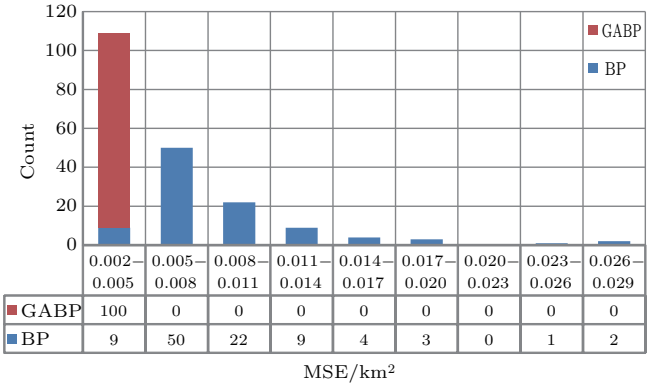


Fig. 9. MSE statistics.

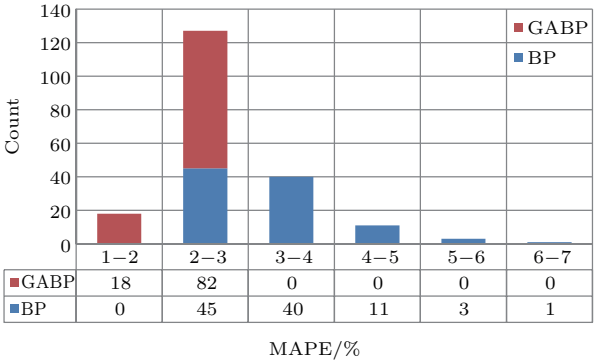


Fig. 10. MAPE statistics.

4. Conclusion and perspectives

In conclusion, a novel GABP technique has been proposed to calculate visibility based on return lidar signals. Belfort visibility datasets are used as standard values to verify the performance of GABP method compared with the traditional inversion and BP methods. Our results demonstrate that the new proposed approach is a significant improvement. The network topology introduced in this study is determined manually. An alternative method for the neural network structure optimization will be part of our future work.

References

[1] Han Y, Gao P, Huang J L, Zhang T X, Zhuang J J, Hu M H and Wu Y H 2018 *Opt. Express* **26** 6833
[2] Kovalev V A and Eichinger W E 2004 *Elastic Lidar: Theory, Practice, and Analysis Methods* (Chichester: John Wiley & Sons)
[3] Klett J D 1981 *Appl. Opt.* **20** 211
[4] Garbarino S, Sorrentino A, Massone A M, Sannino A, Boselli A, Wang X, Spinelli N and Piana M 2016 *Opt. Express* **24** 21497
[5] Kreid D K 1976 *Appl. Opt.* **15** 1823
[6] Button J L and Lyer R S 1978 *Appl. Opt.* **17** 265
[7] Pantazis A, Papayannis A and Georgousis G 2017 *Appl. Opt.* **56** 6440
[8] Xia H Y, Shangguang M J, Wang C, Shentu G L, Qiu J W, Zhang Q, Dou X K and Pan J W 2016 *Opt. Lett.* **41** 5218
[9] Cohen A 1975 *Appl. Opt.* **14** 2878
[10] Fernald F G 1984 *Appl. Opt.* **23** 652
[11] Sun G D, Qin L A, Zhang S L, He F, Tan F F, Jing X and Hou Z H 2018 *Acta Phys. Sin.* **67** 054205 (in Chinese)
[12] Sun G D, Qin L A, Hou Z H, Jing X, He F, Tan F F and Zhang S L 2018 *Opt. Express* **26** 7423
[13] Xia H Y, Shentu G L, Shangguan M J, Xia X X, Jia X D, Wang C, Zhang J, Pelc J S, Fejer M M, Zhang Q, Dou X K and Pan J W 2015 *Opt. Lett.* **40** 1579
[14] Ren C, An N, Wang J Z, Li L, Hu B and Shang D 2014 *Knowl. Based. Syst.* **56** 226
[15] Ding S F, Su C Y and Yu J Z 2011 *Artif. Intell. Rev.* **36** 153
[16] Yu F and Xu X Z 2014 *Appl. Energ.* **134** 102
[17] Sedki A, Ouazar D and Mazoudi E E 2009 *Expert Syst. Appl.* **36** 4523